The Giant Ionospheric Depletion on 15 January 2022 Around the Hunga Tonga-Hunga Ha'apai Volcanic Eruption

Jianhui He, Elvira Astafyeva, Xinan Yue, Feng Ding, Boris Maletckii

The giant ionospheric depletion on 15 January 2022 around the Hunga Tonga-Hunga Ha'apai volcanic eruption

Jianhui He [1, 2, 3, 4], Elvira Astafyeva[4], Xinan Yue [1, 2, 3], Feng Ding[1, 2, 3], Boris Maletckii[4]

1 Key Laboratory of Earth and Planetary Physics, Institute of Geology and Geophysics, Chinese Academy of Sciences, Beijing, China

2 College of Earth and Planetary Sciences, University of Chinese Academy of Sciences, Beijing, China

3 Beijing National Observatory of Space Environment, Institute of Geology and Geophysics, Chinese Academy of Sciences, Beijing, China

4 Université Paris Cité, Institut de Physique du Globe de Paris (IPGP), CNRS UMR 7154, 35-39 Rue Hélène Brion, 75013 Paris, France

Correspondence to: Xinan Yue (yuexinan@mail.iggcas.ac.cn)

Key points:

- The strong (i.e., ~80-95%) and long-lasting (i.e., ~16 hours) ionospheric depletion occurred after the 15 January 2022 Tonga eruption
- The volcanic explosion is responsible for ~60-75% depletion and horizontal extension of ~1500 km
- The depletion was reinforced by the moderate geomagnetic storm, and its extreme duration is due to local night hours

Abstract

The 15 January 2022 Tonga eruption seemed to have caused a strong depletion in the ionospheric electron density. However, the eruption occurred during a moderate geomagnetic storm, so that the depletion could be a local negative effect of the storm. In this work, for the first time, we analyze this depletion and discuss relative contributions of the eruption and the storm through measurements of GNSS-derived vertical total electron content (VTEC), O/N2 ratio by TIMED/GUVI, ion density and temperature by ICON/IVM, and simulations by Thermosphere Ionosphere Electrodynamics General Circulation Model (TIEGCM). We show that shortly after the eruption onset the VTEC in the vicinity of the volcano dropped by ~80-95% below the quiet-time values.The depletion extended up to 4000 km away from the volcano and lasted for ~16 hours, i.e., until local morning hours. Our results suggest that the depletion

was initially caused by the eruption (60-75% negative deviation) and was further reinforced by the storm, by at least 20%. Spatially, only ~1500 km could be attributed to the eruption. This study provides a good illustration of understanding the contributions of forcings from above and below to the ionosphere.

1 Introduction

Ionospheric disturbances driven by natural geological disasters have been extensively discussed by previous studies (Yuen et al., 1969; Tanaka et al., 1984; Heki & Ping, 2005; Heki, 2006; Rolland et al., 2013; Shults et al., 2016; Astafyeva, 2019). Earthquakes, tsunamis or volcanic eruptions generate gravity, gravito-acoustic or shock acoustic waves that propagate upward into the atmosphere and ionosphere. Due to the near-exponential decrease in atmospheric neutral particles with altitude, the corresponding waves can attain rather large amplitudes. Different atmospheric wave modes can be excited and cause ionospheric oscillations in the form of traveling ionospheric disturbances (TIDs) with periodicities in the characteristic frequency domains of infrasonic, acoustic, tsunami-induced gravity waves. These types of waves were observed in the ionosphere by a comprehensive set of satellite and ground-based observations.

On 15 January 2022, one of the most explosive submarine volcanic eruptions in recent years occurred at ~0415 universal time (UT) at the Hunga Tonga-Hunga Ha'apai island (20.54^{o}S, 175.38^{o}W, hereafter "Tonga"). This eruption lasted 11 hours (Witze, 2022) and generated atmospheric shock waves, and also triggered a tsunami that was felt across the Pacific. The eruption also generated numerous disturbances in the ionosphere, i.e., TIDs, that were detected in the vicinity of the volcano and up to 6,000 km away from it (Themens et al., 2022; Zhang et al., 2022; Lin et al., 2022; Maletckii & Astafyeva, 2022).

In addition to the TIDs, the Tonga eruption seemed to cause a huge depletion in the ionospheric total electron content (TEC) in the vicinity of the volcano. Aa et al. (2022) used detrended TEC data and reported a significant local depletion of 5-10 TECU that comprised several cascading TEC decreases. Astafyeva et al. (2022) used unfiltered TEC data and observed the decrease of ~13-18 TECU which represented ~80-90% deviation with respect to the quiet-time reference level. Astafyeva et al. (2022) also reported that the depletion lasted about 1.5-2 hours. They attributed the depletion to the giant shock wave, that was generated by the eruption. Similar ionospheric depletion (also referred to as "ionospheric hole") was

previously observed after large earthquakes (Kakinami et al., 2012; Astafyeva et al., 2013a; Kamogawa et al., 2015) and was explained by strong nonlinear acoustic waves and their impacts (Astafyeva et al., 2011; 2013a; Shinagawa et al., 2013; Zettergren & Snively, 2015). However, the Tonga-related depletion seemed to be much stronger than the earthquake-generated ionospheric holes. Astafyeva et al. (2022) suggested that the eruption-driven hole was reinforced by a moderate geomagnetic storm that was ongoing during the eruption. However, up to now, no detailed analysis was performed and the depletion was fully attributed to the eruption. In addition, the depletion itself has not yet been investigated in detail. In addition, we note that the datasets that were used previously by Aa et al. (2022) and Astafyeva et al. (2022) do not allow to estimate the true magnitude and duration of the depletion. The use of detrending procedure or band-pass filter removes the depletion from TEC data series and alters its magnitude. While, the use of relative TEC time series can only provide relative amplitude of the depletion, and the duration of the depletion observation is compromised by the limited duration of observations by GNSS receivers.

In this work, for the first time, we provide a detailed study of the Tonga ionospheric depletion. We use global maps of the absolute vertical TEC along with O/N2 data from the Thermosphere, Ionosphere, Mesosphere Energetics and Dynamics/Global Ultraviolet Imager (TIMED/GUVI), and ion density and temperature from the Ionospheric Connection Explorer (ICON) Ion Velocity Meter, to illustrate the ionosphere and thermosphere disturbance during this period. In addition, the model simulation results from the National Center for Atmospheric Research (NCAR) Thermosphere Ionosphere Electrodynamics General Circulation Model (TIEGCM) are further used to determine thermospheric/ionospheric variations during the geomagnetic storm.

2 Data and Methods

The two-dimensional vertical total electron content (VTEC) observations are provided by the Massachusetts Institute of Technology's (MIT) Haystack Observatory with a 1° by 1° bin in latitude and longitude and a 5-min time resolution (Rideout & Coster, 2006). To investigate spatio-temporal variations, here we analyse VTEC maps for three days, from 14 to 16 January 2022. To retrieve the depletion, we subtract the reference values from the event data. The reference is calculated by averaging data over 4 quiet days: 10, 11, 12 and 13 January 2022.

The thermospheric O/N2 ratio measurements are provided by the Thermosphere, Ionosphere, Mesosphere Energetics and Dynamics/Global Ultraviolet Imager (TIMED/GUVI)

with 74.1° inclination and a 97.8 min period (Stephan et al., 2008). This ratio is widely used in the ionospheric storm analysis as an indicator of a neutral composition disturbance (Christensen et al., 2003; Meier et al., 2005; Crowley et al., 2006).

The ionosphere ion density and temperature measurements are provided by the Ionospheric Connection Explorer Ion Velocity Meter (ICON/IVM) with 27^{o} inclination and 575 km height (Immel et al., 2018). These datasets provide a unique opportunity to analyze the spatio-temporal ionosphere disturbance in the vicinity of Tonga.

The model simulation results of storm-related ionosphere and thermosphere effects are from the National Center for Atmospheric Research Thermosphere Ionosphere Electrodynamics General Circulation Model (TIEGCM). In this study, we used the high-resolution model version with 1.25°x1.25° in geographic latitude and longitude, and a vertical resolution of 1/4 scale height (Dang et al., 2018). The Weimer empirical model (Weimer, 2005), driven by the realistic interplanetary and solar/magnetic indices, including the daily and 81-day average F10.7 cm solar flux, solar wind velocity and proton number density, and interplanetary magnetic field Bx, By and Bz components, was used to specify the high-latitude ion convection pattern. These space weather indices are provided in Figure S1 in Supplementary Information. At the model lower boundary, atmospheric migrating tides are specified by the Global Scale Wave Model (GSWM) (Hagan & Forbes, 2003). Note that no volcano-related effects are included in this model. The simulation results used in this paper include the TEC and O/N2 ratio.

3 Results and Discussions

Figure 1 (a) shows the time evolution of the two-dimensional differential VTEC maps from 0417 to 2317 UT on 15 January 2022 in the vicinity of the Tonga volcano. The full world coverage for 14-16 January can be found in Animation S1 in Supplementary Information. Figure 1 (a) clearly shows negative deviation of the VTEC around the volcano starting from 0437 UT, i.e., ~20 minutes after the beginning of the eruption. The depletion further seemed to propagate away from the volcano to as far as 3000 km distance at around 0637 UT, and ~4000 km at around 0717 UT. We also note that the depletion seemed to be stronger on the south-western side from the volcano. However, only a few observation points are available eastward from the volcano to better confirm this asymmetry. The maximum depletion of -24 TECU (i.e., 95% as compared to the before-eruption value of 26 TECU, Figure S2) can be observed at ~0617-0637 UT on the south-west from the volcano, near -30^{o}S.

From 1217 UT, the depletion decreased in value and in spatial coverage, and it ended at around 2017 UT, i.e. during local morning hours. Therefore, this great depletion lasted for ~16 hours. Similar conclusions about the depletion's duration and magnitude can be done from the time series of the absolute VTEC (Figure S2).

To further prove the spatial and temporal of the observed depletion with the volcanic eruption, Figure 2 shows VTEC keograms for the volcano longitude (175.38^{o}W) and latitude (20.55^{o}S) for the period 14-16 January 2022. From Figures 2a and 2b, it follows that no depletion occurred on 14 January. On 15 January, we first see a small -2 TECU deviation between 0200 and 0400UT. However, starting from ~0430 UT the TEC strongly depleted at the volcano latitude, and it further moved away from the volcano with time in both northern and southern directions (Figure 2a). The depletion seems to have an asymmetric pattern after ~0600 UT, as it extends in southern (poleward) direction. From 1300 UT, the TEC comes closer to the reference values, but a smaller -4 TECU depletion persists until ~2000 UT.

Along the volcano latitude, very pronounced TEC depletion occurred at the volcano longitude starting from ~0430 UT (Figure 2b). Further, from ~0430 to ~0600 UT, the depletion clearly propagates in both western and eastern directions even though very few data points were available in the eastern direction. The maximum depletion of -21 TECU (i.e., ~80% of the before-eruption level) occurred around 0600 UT. These depleted percentage changes can also be confirmed in Figure S2. After that, the depletion only can be seen eastward from the volcano. The largest longitude extension was near 160^{o}E. Finally, it became less visible at 2000 UT.

Based on these keograms, we can roughly estimate that shortly after the eruption onset, the depletion propagated at ~200 ms^{-1} in meridional direction and ~280 ms^{-1} in zonal direction. Besides, a travel-time diagram of the north-south differential VTEC from the volcano center position is also represented in Figure S3 in Supplementary Information. The existence of ionospheric holes can be clearly recognized. This confirmed that the observed large-scale depletion was related to the volcanic eruption.

However, we note that a keogram for 16 January shows that very similar TEC depletion, although of smaller amplitude, occurs around the same time intervals (e.g., ~0400-2000 UT) as that shown on 15 January southward from the volcano. This phenomenon can also be confirmed in two-dimensional differential VTEC maps for 16 January (Figure S4 in Supplementary Information). Therefore, the 15 January large-scale depletion was, most likely, not fully generated by the volcanic eruption, but, at least partly, was due to a geomagnetic storm that was ongoing during the eruption. The storm commenced at ~1600 UT on 14 January 2022 (Figures S1 and 2c). The main phase lasted for about 7 hours from 1600 to 2200 UT. The

minimum Dst index dropped to -91 nT, and the maximum Kp index went up to 6 at 2200 UT on 14 January 2022 (Figure S1 in Supplementary Information). Then, a long-lasting recovery phase started on 15 January, i.e., the explosive Tonga volcanic eruption occurred at the early stage of the storm's recovery phase.

Geomagnetic storms are known to produce positive and negative variations (often referred to as positive and negative ionospheric storms) in the ionospheric parameters driven by storm-time alterations in the electric field, neutral winds and thermospheric composition. The negative storm effects are often reported during the storm recovery phase due to the occurrence of regions with decreased neutral composition ratio O/N2. Such regions are originally produced due to heating and upwelling of the lower thermosphere by the magnetospheric energy inputs at auroral latitudes. They are further pushed to lower latitudes by the equatorward thermospheric winds or traveling atmospheric disturbances (Fuller-Rowell et al., 1996). The O/N2 ratio has a highly positive correlation with ionospheric electron density, with a(n) increase/decrease of the ionosphere electron density as the O/N2 ratio increases/decreases (Prölss, 1976, 1980; Fuller-Rowell et al., 1994; Strickland et al., 2001; Christensen et al., 2003; Crowley et al., 2006).

Figure 3a shows the O/N2 ratio on 14-16 January 2022 as observed by the TIMED/GUVI satellite (top panel), and as modeled by the TIEGCM and interpolated to the location of the satellite based on the model gridded value (bottom panel). The TIMED satellite passed around the Tonga volcano at ~17.70 UT on 14 January, i.e. before the eruption but during the storm, and at ~17.90 UT on 15 January, i.e. several hours after the eruption stopped, but when the TEC was yet depleted. The decreased O/N2 bulge first occurred at high latitudes during the main phase of the storm, and it started to extend to middle latitudes at ~2100 UT on 14 January (Figure 3a). On 15 January, the bulge further stretched to low latitudes and covered the Pacific and Australian regions. From these TIMED/GUVI observations we conclude that the composition was depleted around the volcano area during the TEC depletion observation.

With regard to the TIEGCM O/N2 simulations, they differ from the observations in the absolute O/N2 value and in the O/N2 disturbance around the volcano area (Figure 3a). While, the relative morphology variations and the O/N2 disturbance over the Western Australia are correctly simulated. Therefore, we will use them to further investigate the O/N2 ratio changes during the storm. Figure 3 b shows the differential O/N2 simulated by the TIEGCM. At 2000 UT on 14 January, the O/N2 depletion occurred in the Australian region, which is consistent with the TIMED/GUVI observations. The O/N2 depletion further enhanced and was the strongest at 0400UT on 15 January, i.e. during the beginning of the eruption. The composition

remained locally decreased until at least 0400UT on 16 January. Besides, Figure 3a and 3b show that a higher O/N2 depletion level occurred on 15 January than that on 16 January, which is in line with VTEC observations depletion on 15-16 January (Figure 2a-b).

Figure 3c further shows the observed and TIEGCM-simulated differential VTEC comparison for different longitudes and at the volcano latitude for 14-16 January. The global view of the observed and simulated ionosphere negative storm effects in VTEC can be found in Animation S1 in Supplementary Information. From Figure 3c, one can see that the TIEGCM can generally reproduce the negative TEC storm effects due to the storm-time decreased O/N2, especially at 0400-2000 UT on 15 January (the yellow shading). Note that the 85^{o} and 105^{o} longitudes are not shown here due to the absence of observations. The simulated VTEC changes for four longitudes near the volcano have been calculated to estimate the storm's contribution. For 145^{o} longitude, the TEC dropped down to -4.35 TECU around 0800 UT on 15 January, which represents 28% with respect to the background level. We further observe -3.45 TECU (23.6%) at 155^{o}, -2.14 TECU (15.5%) at 165^{o}, and -0.93 TECU (7.6%) at 175^{o}. Note that the simulated O/N2 depletion does not occur over the volcano (shown in Figure 3a), and the model did not correctly simulate the VTEC evolution in this region. While, as indicated above, the relative morphology variations in O/N2 ratio are much better simulated in the Australian region. Therefore, the TEC changes at 155^{o} correctly represent the storm contribution, which is -3.45 TECU (23.6%). Considering that the storm-time effects around the volcano area should be similar to those in the Australian region, we estimate the storm contribution to be at least 20%. Consequently, the true contribution of the eruption should be about 60-75%, which remains an impressive number.

The true magnitude of the depletion can also be understood from Figure 4 that presents the difference of the ΔVTEC between 15 and 16 January and the ICON/IVM ion density and ion temperature measurements. Note, however, that the storm-driven depletion on 16 January was smaller than that on 15 January, therefore, the differential VTEC between 15 and 16 January still contains a small storm effect in addition to the eruption effect. The differential VTEC maps show the ΔVTEC deviation of -15 to -20 TECU, which represents 60-75% of the background level and is in line with our previous estimations. The true horizontal dimensions can also be seen in Figure 4, as we see the depletion extension up to 1500-2000 km on the west-south-west. While, the depletion ~3000-4000 km south-west from the volcano seen in Figure 1 should be due to the storm.

The significant local depletion around the volcano is also seen in the ion density at 575 km as measured by ICON (Figure 4). One can see strong decreases in the ion density (by 1-2 orders

of magnitude) and noticeable increases in the ion temperature (by 500-1000 K) at $\pm 15^{\circ}$ from the volcano. These local effects confirmed that only ~1500 km away from the epicenter is attributed to the eruption. We note that the depletion was only seen from 0637 UT to 1657 UT, when the satellite passed close to the volcano. The satellite is away from the epicenter at 1837 UT and 2022 UT, but smaller negative deviation is actually well seen in differential VTEC, i.e. until local morning hours.

The exact mechanism of the generation of the ionospheric depletion by the eruption is not yet clear. Aa et al. (2022) suggested that the TEC depletion was more likely to be caused by strong expansion and upwelling in the thermosphere along with outward ionospheric plasma flow driven by impulsive nonlinear acoustic wave pulses. Astafyeva et al. (2022) attributed the depletion to the giant shock wave that was generated by the volcanic explosion, however, no detailed investigation was performed. Similar depletions although of much smaller amplitude were previously reported for several large earthquakes (Kakinami et al., 2012; Astafyeva et al., 2013a; Kamogawa et al., 2015). For instance, the 2011 Tohoku earthquake caused a depletion of magnitude -5-6 TECU that only lasted 30-50 min (Astafyeva et al., 2011; 2013 a, b; Kakinami et al., 2012). Simulation studies by Shinagawa et al. (2013) and Zettergren et al. (2017) for the 2011 Tohoku-oki earthquake demonstrated that the ionospheric TEC depletion can be formed by large-magnitude earthquakes that generate strong-amplitude, and therefore non-linear acoustic waves. Additionally, Zettergren et al. (2017) showed that such depletions are further reinforced by the uplifted gas that falls back and causes the incoming acoustic waves to slow as they propagate upward (since they are propagating in a falling background medium). As a result, these incoming wave fronts then dissipate more within the F region. For waves with large amplitudes, the slowed incoming wave fronts then may partly or fully merge with the next set of wave fronts that follow. The combined impact of these non-linear acoustic waves and dissipated processes is mostly the strong downward neutral velocity, which generates a downward, field-aligned motion in the ionospheric plasma through ion-neutral drag. The effect of the downward motion will tend to result in enhanced ionospheric O^+ recombination due to the plasma is transported to an altitude where molecular constituents (e.g., N_2) are denser. Then, the effect of this motion is a conversion of O^+ into molecular ions. It is known that molecular ions recombine more readily than O^+. These net effects result in a TEC depletion that persists longer than the associated thermospheric dynamics.

The exceptionally long duration of the Tonga depletion could be explained by very intensive shock wave that was generated by the volcanic explosion as compared to earthquakes,

and by the local evening and night hours which should have hindered faster recovery from low ionization.

Besides, the longer depletion could have been additionally reinforced and prolonged by chemical effects due to the eruption. Millán et al. (2022) reported that the Tonga eruption-driven ash plume and water vapor reached as high as 39 to 55 km of altitude, i.e. the mesosphere layer. If this water vapor could further be transported to the ionospheric altitudes, at least partly, it could cause an increase in the recombination rate, leading to a significant decline in ionospheric Ne (e.g., Mendillo & Forbes, 1978). The simultaneous process of the molecule diffusion and the dissociative recombination cause the formation of an "ionospheric hole". Specifically, the diffusion of molecule density in the exhaust plume at a certain radial distance from a point source can be assumed as a spherical diffusion. The diffusion constant is larger with a higher altitude. The water and hydrogen molecules become positive molecular ions by reacting with ambient oxygen ions. Then, their dissociative recombination with electrons led to the depletion of the ionospheric electron density. This effect has been confirmed by depletion caused by launches of missile and rockets launches (Furuya & Heki, 2008; Ozeki & Heki, 2010).

Future studies, especially modelling, will help to better explain this observed effect.

4 Conclusions

In this work, for the first time, we presented a detailed analysis of the ionospheric depletion that occurred shortly after the 15 January 2022 giant explosive eruption of the Hunga-Tonga volcano. As the eruption began at ~0415 UT on 15 January, the TEC dropped by ~80-95% with respect to quiet-time values. Such negative effect lasted for ~16 hours, i.e., until local morning hours. On VTEC maps, the depletion extended up to ~4000 km away from the epicenter. Additionally, ICON-IVM measurements showed significant decrease in the ion density at 575 km of altitude in the vicinity of the volcano.

The depletion occurred during the recovery phase of a moderate geomagnetic storm, and storms are known to produce local decreases and increases of ionospheric plasma density. Therefore, we analysed storm-time effects and we found that the decrease in thermospheric neutral compositions ratio O/N2 was responsible for ionospheric negative storm effects at middle and low latitudes in the Australian and Pacific regions. This storm effect in the ionosphere and thermosphere can also be well reproduced by the TIEGCM simulation.

Both observations and simulations suggest that the depletion was initially generated by the

volcanic explosion (~60-75% contribution and ~1500 horizontal spatial extent) and was by ~20% reinforced by the thermospheric composition changes due to a moderate geomagnetic storm.

5 Open Research

The MIT VTEC data are publicly available at the Madrigal Database (http://cedar.openmadrigal.org/). The thermospheric O/N2 composition data are available from: http://guvitimed.jhuapl.edu/guvi-galleryl3on2. The space weather indices are derived from OMNIWeb database (http://omniweb.gsfc.nasa.gov/). The ICON/IVM ion density and temperature data can be accessed at (https://icon.ssl.berkeley.edu/Data). The TIEGCM simulations presented in this paper can be accessed from Open Science Framework (https://doi.org/10.17605/OSF.IO/YAVXN).

6 Acknowledgement

This work was supported by the French Space Agency (CNES), project "RealDetect", the Project of Stable Support for Youth Team in Basic Research Field, CAS (YSBR-018), the International Partnership Program Of Chinese Academy of Sciences (Grant No. 183311KYSB20200003), the National Natural Science Foundation of China (42104160), and the China Scholarship Council (CSC). We thank L. Rolland, P. Coïsson, F. Manta, D. Mikesell, E. Munaibari & M. Ravanelli for fruitful discussions within an ad-hoc Geoazur-IPGP-NGI working group on the 2022 Hunga Tonga volcano eruption.

References

Aa, E., Zhang, S.-R., Erickson, P. J., Vierinen, J., Coster, A. J., Goncharenko, L. P., et al. (2022). Significant ionospheric hole and equatorial plasma bubbles after the 2022 Tonga volcano eruption. *Space Weather*, 20, e2022SW003101. https://doi.org/10.1029/2022SW003101

Astafyeva, E. (2019). Ionospheric detection of natural hazards. *Reviews of Geophysics*, 57(4), 1265-1288. https://doi.org/10.1029/2019RG000668

Astafyeva, E., B. Maletckii, T.D. Mikesell, E. Munaibari, M. Ravanelli, P. Coisson, F. Manta, L. Rolland. (2022). The 15 January 2022 Hunga Tonga eruption history as inferred from

ionospheric observations. *Geophysical Research Letters*, https://doi.org/10.1029/2022GL098827

Astafyeva, E., L. Rolland, P. Lognonné, K. Khelfi, T. Yahagi. (2013b). Parameters of seismic source as deduced from 1Hz ionospheric GPS data: case-study of the 2011 Tohoku-oki event. *Journal of Geophysical Research: Space Physics*, V. 118, 9, 5942-5950, doi:10.1002/jgra50556

Astafyeva, E., P. Lognonné, and L. Rolland. (2011) First ionosphere images for the seismic slip on the example of the Tohoku-oki earthquake. *Geophysical Research Letters*, V.38, L22104, doi:10.1029/2011GL049623.

Astafyeva, E., Shalimov, S., Olshanskaya, E., Lognonné, P. (2013a). Ionospheric response to earthquakes of different magnitudes: larger quakes perturb the ionosphere stronger and longer. *Geophysical Research Letters*, V.40, N9, 1675-1681, doi: 10.1002/grl.50398

Christensen, A. B., Paxton, L. J., Avery, S., Craven, J., Crowley, G., Humm, D. C., et al. (2003). Initial observations with the Global Ultraviolet Imager (GUVI) in the NASA TIMED satellite mission. *Journal of Geophysical Research: Space Physics*, 108(A12), 1451, https://doi.org/10.1029/2003JA009918

Crowley, G., Hackert, C. L., Meier, R. R., Strickland, D. J., Paxton, L. J., Pi, X., et al. (2006). Global thermosphere-ionosphere response to onset of 20 November 2003 magnetic storm. *Journal of Geophysical Research: Space Physics*, 111, A10S18, https://doi.org/10.1029/2005JA011518

Dang, T., Lei, J., Wang, W., Burns, A., Zhang, B., & Zhang, S.-R. (2018). Suppression of the polar tongue of ionization during the 21 August 2017 solar eclipse. *Geophysical Research Letters*, 45, 2918–2925. https://doi.org/10.1002/2018GL077328

Furuya, T., & K. Heki. (2008). Ionospheric hole behind an ascending rocket observed with a dense GPS array. *Earth Planets Space*, 60, 235–239

Fuller-Rowell T. J., Codrescu, M. V., Rishbeth, H., Moffett, R.J., & Quegan, S. (1996). On the seasonal response of the thermosphere and ionosphere to geomagnetic storms. *Journal of Geophysical Research: Space Physics*, 101(A2):2343–2353, doi:10.1029/95JA01614

Fuller-Rowell, T. J., Codrescu, M. V., Moffett, R. J., & Quegan, S. (1994). Response of the thermosphere and ionosphere to geomagnetic storms. *Journal of Geophysical Research: Space Physics*, 99(A3), 3893–3914, https://doi.org/10.1029/93JA02015

Hagan, M. E., & Forbes, J. M. (2003). Migrating and nonmigrating semidiurnal tides in the upper atmosphere excited by tropospheric latent heat release. *Journal of Geophysical Research: Space Physics*, 108(A2), 1062, https://doi.org/10.1029/2002JA009466

Heki, K., & Ping, J. (2005). Directivity and Apparent Velocity of the Coseismic Ionospheric Disturbances Observed with a Dense GPS Array. *Earth and Planetary Science Letters*, 236, 845–855, doi:10.1016/j.epsl.2005.06.010

Heki, K. (2006). Explosion energy of the 2004 eruption of the Asama Volcano, central Japan, inferred from ionospheric disturbances. *Geophysical Research Letters*, 33, L14303, doi:10.1029/2006GL026249

Immel, T. J., England, S. L., Mende, S. B., Heelis, R. A., Englert, C. R., Edelstein, J., et al. (2018). The ionospheric connection explorer mission: Mission goals and design. *Space Science Reviews*, 214(1), 13. https://doi.org/10.1007/s11214-017-0449-2

Kakinami, Y. et al. (2012). Tsunamigenic ionospheric hole. *Geophysical Research Letters*, 39, L00G27, doi:10.1029/2011GL050159

Kamogawa, M. et al. (2015), Does an ionospheric hole appear after an inland earthquake?. *Journal of Geophysical Research: Space Physics*, 120, 9998–10,005, doi:10.1002/2015JA021476

Lin, J.-T., Rajesh, P. K., Lin, C. C. H., Chou, M.-Y., Liu, J.-Y., Yue, J., Hsiao, T.-Y., Tsai, H.-F., Chao, H.-M., & Kung, M.-M. (2022). Rapid conjugate appearance of the giant ionospheric Lamb wave signatures in the northern hemisphere after Hunga Tonga volcano eruptions. *Geophysical Research Letters*, 49, e2022GL098222, https://doi.org/10.1029/2022GL098222

Maletckii, B., & Astafyeva, E. (2022). Near-real-time analysis of the ionospheric response to the 15 January 2022 Hunga Tonga-Hunga Ha'apai volcanic eruption. *Journal of Geophysical Research: Space Physics*, 127, e2022JA030735. https://doi.org/10.1029/2022JA030735

Meier, R. R., Crowley, G., Strickland, D. J., Christensen, A. B., Paxton, L. J., Morrison, D., & Hackert, C. L. (2005). First look at the 20 November 2003 superstorm with TIMED/GUVI: Comparisons with a thermospheric global circulation model. *Journal of Geophysical Research: Space Physics*, 110, A09S41, https://doi.org/10.1029/2004JA010990

Mendillo & Forbes. (1978). Artificially created holes in the ionosphere. *Journal of Geophysical Research: Space Physics*, 83, A01, https://doi.org/10.1029/JA083iA01p00151

Millán, L., Santee, M. L., Lambert, A., Livesey, N. J., Werner, F., Schwartz, M. J., et al. (2022). The Hunga Tonga-Hunga Ha'apai Hydration of the Stratosphere. *Geophysical Research Letters*, 49, e2022GL099381. https://doi.org/10.1029/2022GL099381

Ozeki & Heki. (2010). Ionospheric holes made by ballistic missiles from North Korea detected with a Japanese dense GPS array. *Journal of Geophysical Research: Space Physics*, 115, A09, https://doi.org/10.1029/2010JA015531.

Prölss, G. W. (1976). On explaining the negative phase of ionospheric storms. *Planetary and Space Science*, 24, 607-609

Prölss, G.W. (1980). Magnetic Storm Associated Perturbations of the Upper Atmosphere: Recent Results Obtained by Satellite-Borne Gas Analyzers. *Reviews of Geophysics*, V.18, N1, 183-202

Rideout, W., & A. Coster. (2006). Automated GPS processing for global total electron content data. *GPS Solutions*, 10, 219–228, doi:10.1007/S10291-006-0029-5

Rolland, L. M., M. Vergnolle, J.-M. Nocquet, A. Sladen, J.-X. Dessa, F. Tavakoli, H. R. Nankali, & F. Cappa. (2013). Discriminating the tectonic and non-tectonic contributions in the ionospheric signature of the 2011, Mw7.1, dip-slip Vanearthquake, Eastern Turkey. *Geophysical Research Letters*, 40, 378, doi:10.1002/grl.50544

Shinagawa, H., T. Tsugawa, M. Matsumura, T. Iyemori, A. Saito, T. Maruyama, H. Jin, M. Nishioka, & Y. Otsuka. (2013). Two-dimensional simulation of ionospheric variations in the vicinity of the epicenter of the Tohoku-oki earthquake on 11 March 2011. *Geophysical Research Letters*, 40, 5009–5013, doi:10.1002/2013GL057627

Shults, K., E. Astafyeva & S. Adourian. (2016). Ionospheric detection and localization of volcano eruptions on the example of the April 2015 Calbuco events. *Journal of Geophysical Research: Space Physics*, V.121, N10, 10,303-10,315, doi:10.1002/2016JA023382

Stephan, A. W., Meier, R. R., & Paxton, L. J. (2008). Comparison of Global Ultraviolet Imager limb and disk observations of column O/N2 during a geomagnetic storm. *Journal of Geophysical Research: Space Physics*, 113, A01301, https://doi.org/10.1029/2007JA012599

Strickland, D. J., R. E. Daniell, & J. D. Craven. (2001). Negative ionospheric storm coincident with DE-1 observed thermospheric disturbance on October 14, 1981. *Journal of Geophysical Research: Space Physics*, 106, 21,049, doi:10.1029/2000JA000209.

Tanaka, T., T. Ichinose, T. Okuzawa, T. Shibata, Y. Sato, C. Nagasawa, & T. Ogawa. (1984). HF-Doppler observations of acoustic waves excited by the Urakawa-Oki earthquake on 21 March 1982. *Journal of Atmospheric and Terrestrial Physics*, 46(3), 233– 245.

441 Themens, D. R., Watson, C., Žagar, N., Vasylkevych, S., Elvidge, S., McCaffrey, A., et al.
442 (2022). Global propagation of ionospheric disturbances associated with the 2022 Tonga
443 volcanic eruption. *Geophysical Research Letters*, 49, e2022GL098158,
444 https://doi.org/10.1029/2022GL098158
445 Weimer, D. R. (2005). Predicting surface geomagnetic variations using ionospheric
446 electrodynamic models. *Journal of Geophysical Research*, 110, A12307,
447 doi:10.1029/2005JA011270
448 Witze, A. (2022). Why the Tongan eruption will go down in the history of volcanology.
449 *Nature*, 602, 376-378, doi:https://doi.org/10.1038/d41586-022-00394-y
450 Yuen, P. C., P. F. Weaver, R. K. Suzuki, & A. S. Furumoto. (1969). Continuous, traveling
451 coupling between seismic waves and the ionosphere evident in May 1968 Japan
452 earthquake data. *Journal of Geophysical Research: Space Physics*, 74(9), 2256– 2264
453 Zettergren, M. D., & Snively, J. B. (2015). Ionospheric Response to InfrasonicAcoustic Waves
454 Generated by Natural hazard Events. *Journal of Geophysical Research: Space Physics*,
455 120, 8002–8024, doi:10.1002/2015ja021116
456 Zettergren, M. D., J. B. Snively, A. Komjathy, and O. P. Verkhoglyadova. (2017). Nonlinear
457 ionospheric responses to large-amplitude infrasonic-acoustic waves generated by
458 undersea earthquakes. *Journal of Geophysical Research: Space Physics*, 122, 2272–2291,
459 doi:10.1002/2016JA023159
460 Zhang S-R, Vierinen J, Aa E, Goncharenko LP, Erickson PJ, Rideout W, Coster AJ and Spicher
461 A. (2022). 2022 Tonga Volcanic Eruption Induced Global Propagation of Ionospheric
462 Disturbances via Lamb Waves. *Frontiers in Astronomy - and Space Sciences*, 9:871275.
463 doi: 10.3389/fspas.2022.871275
464

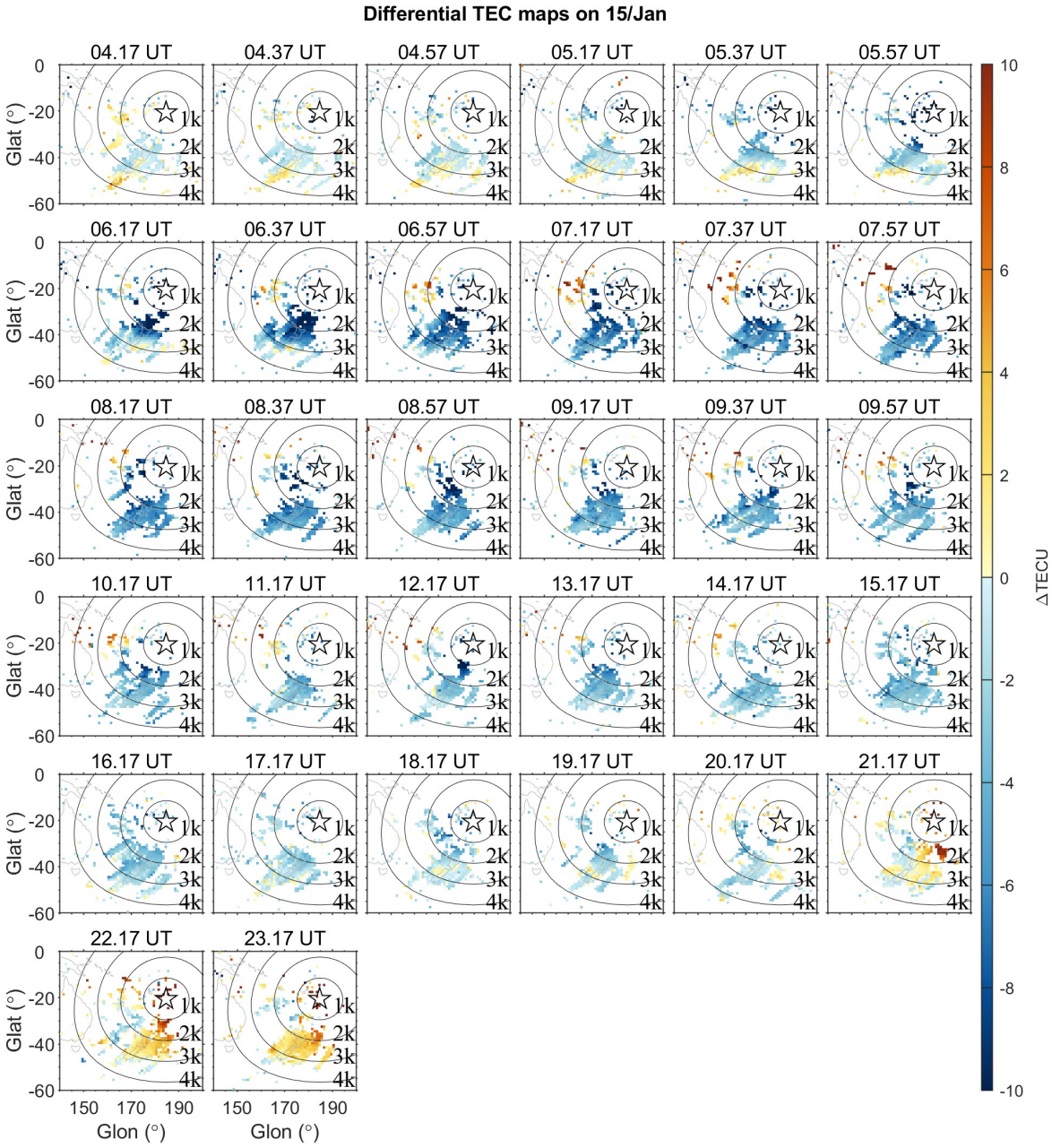

Figure 1 The two-dimensional differential VTEC maps for the near-volcano area at different universal times on 15 January 2022. The volcano eruption location is marked by the pentagram. The iso-distance circles from the eruption epicenter are shown in dark solid lines (unit: km). The differential TEC indicates the deviation of the TEC value on 15 January from the reference value. The reference value is the averaged data over 4 quiet days: 10, 11, 12 and 13 January 2022.

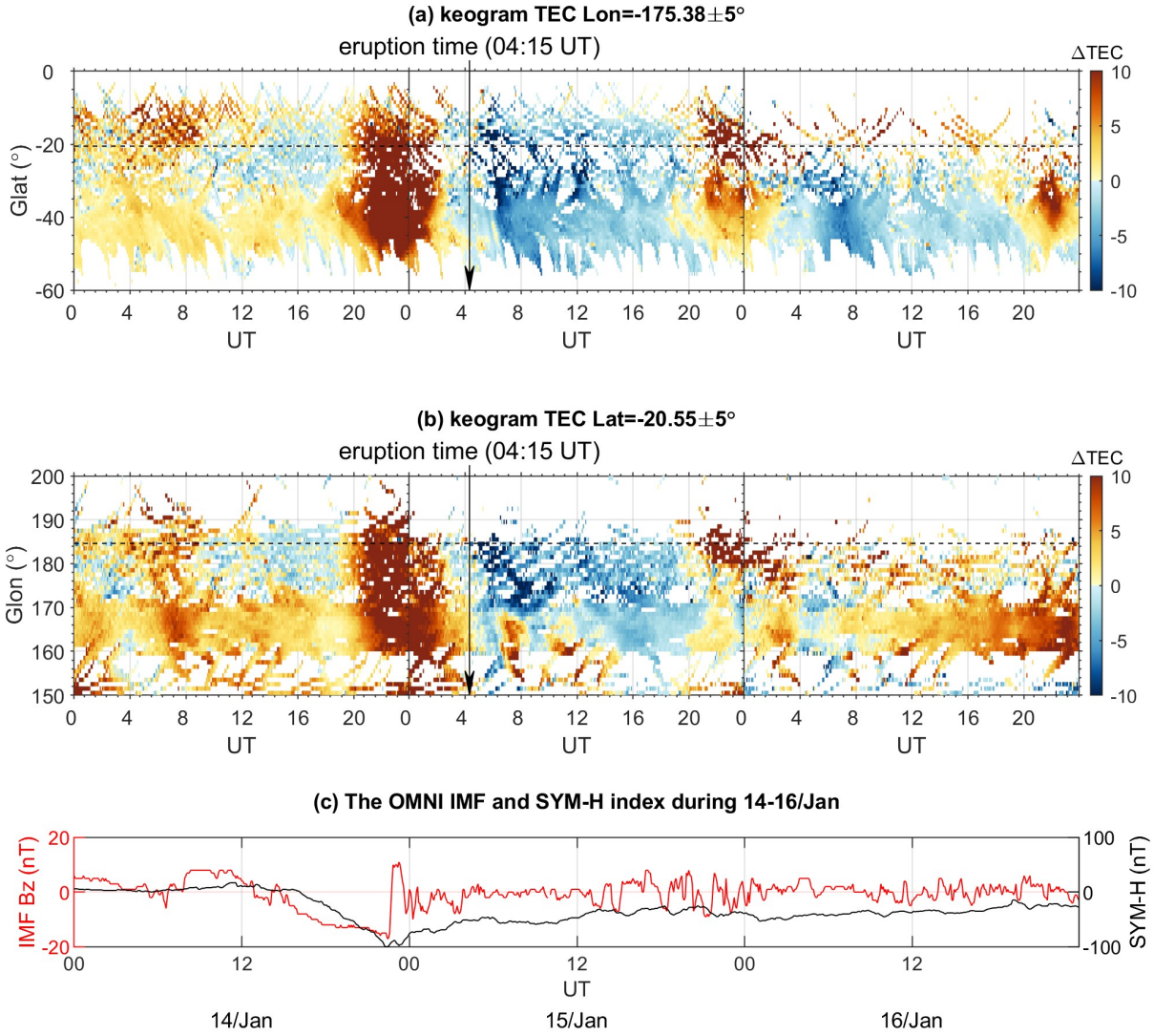

Figure 2 The time evolution of the differential VTEC at a fixed longitude (a) and latitude (b) near-volcano location during the whole day of 14-16 January 2022. The dark dashed lines indicate the latitude and longitude of the Tonga volcano. The arrows indicate the eruption time at 0415 UT on 15 January 2022. (c) The interplanetary magnetic field (IMF) Bz component (red line) and SYM-H index (black line) from the OMNI dataset with 5-min resolution for 14-16 January 2022.

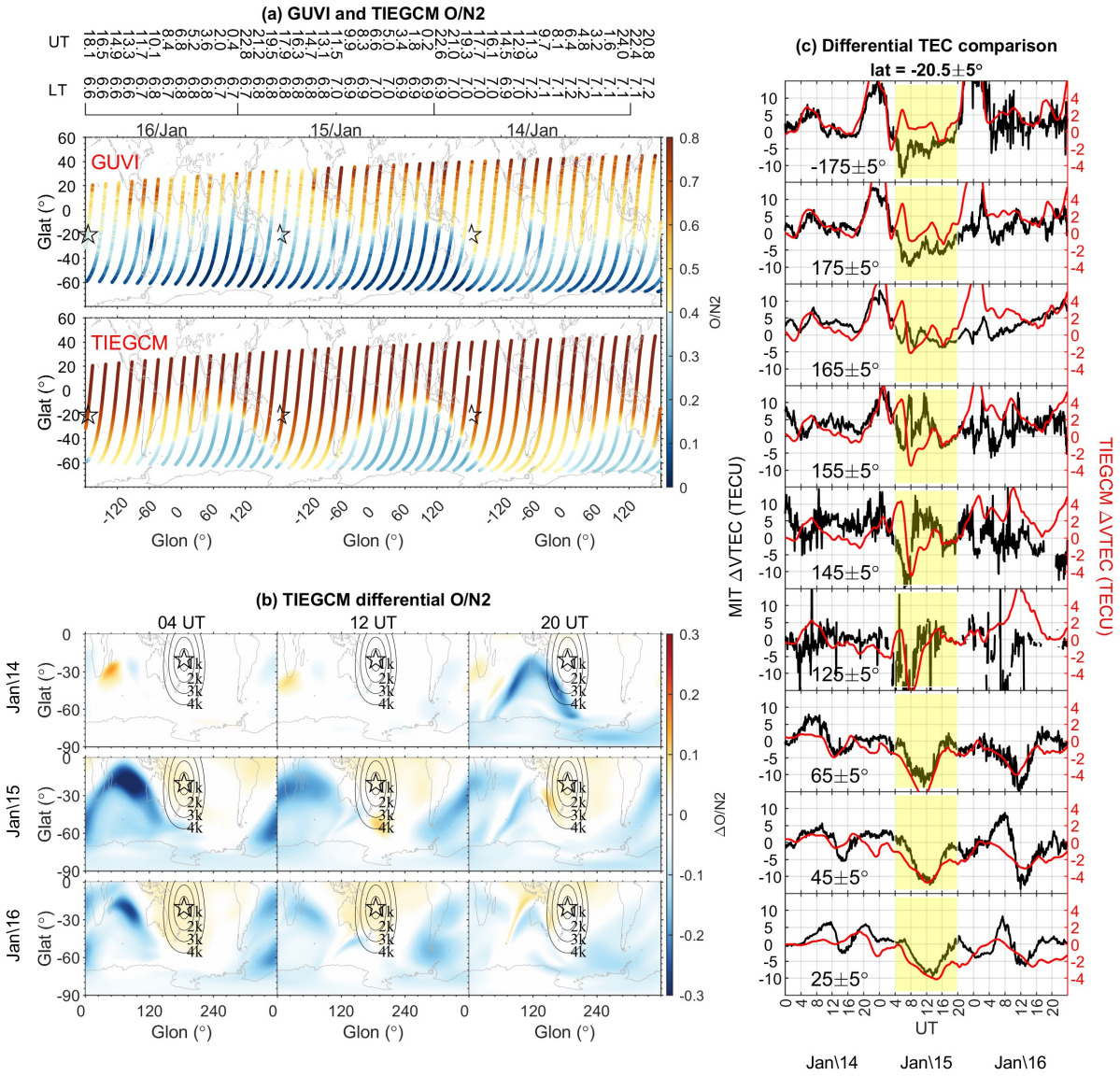

Figure 3 (a) The thermospheric O/N2 ratio as measured by the TIMED/GUVI satellite (top) and modeled by TIEGCM (bottom) on 14-16 January 2022 in the local early morning sector (6.6-7.2 LT). The universal times and local times of the equator crossings for each orbit are indicated on the top. The pentagram indicates the volcano eruption location. (b) The longitude-latitude distribution of the TIEGCM differential O/N2 ratio in southern hemisphere at 0400 UT, 1200 UT and 2000 UT on 14-16 January. The differential O/N2 ratio indicates the deviation of the O/N2 value on 14-16 January from the reference value on 13 January. The iso-distance circles from the eruption epicenter are shown in dark solid lines (unit: km). (c) The differential TEC comparison between MIT VTEC (black lines) and TIEGCM (red lines) for different longitudes at a fixed latitude near-volcano location on 14-16 January 2022. The yellow shading indicates the period of TEC depletion observation, i.e. 0400 to 2000 UT on 15 January 2022.

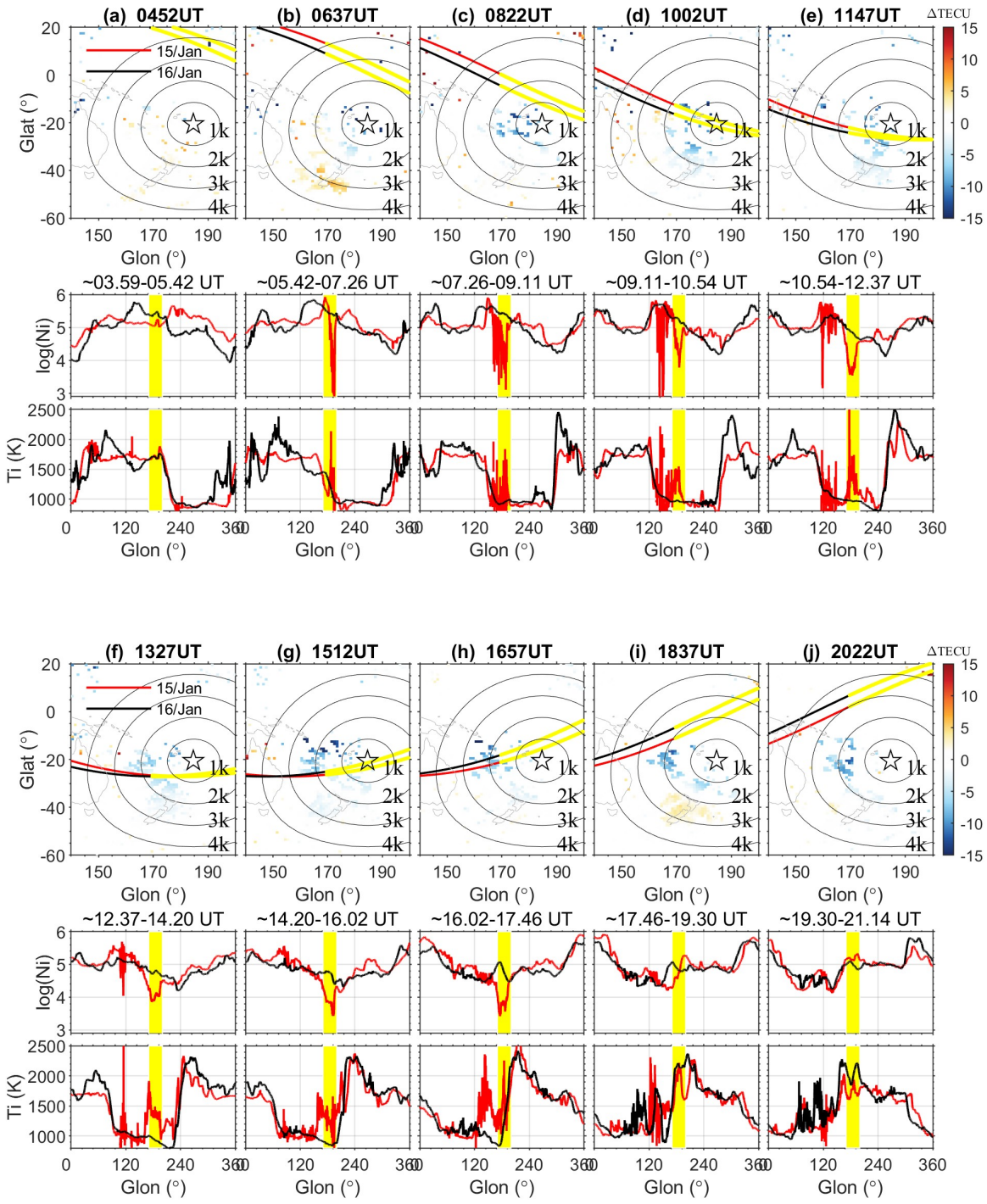

Figure 4 (a-j) The top panels: The two-dimensional differential VTEC maps between 15 and 16 January on the near-volcano area at different universal times. The ICON-IVM observation tracks near volcano area are shown in red and dark thick solid lines on 15 and 16 January, respectively. The volcano eruption location is marked by the pentagram. The iso-distance circles from the eruption epicenter are shown in dark thin solid lines (unit: km). The middle and

499 bottom panels: The ICON-IVM ion density and ion temperature measurements at different
500 universal times on 15-16 January. The red and black thick solid lines indicate the ion density
501 and ion temperature on 15 and 16 January, respectively. Note that the yellow part of each trace
502 and the yellow shading of each subpanel indicate the volcano location within $\pm 15^{\circ}$.